Concurrent Trajectory Optimization and Aircraft Design for the Air Cargo Challenge 2022 Competition

Nuno Miguel Bento de Matos
nuno.matos@tecnico.ulisboa.pt

Instituto Superior Técnico, Universidade de Lisboa, Portugal

December 2021

Abstract

In this work, a coupled aerostructural aircraft design and trajectory optimization framework is developed for the Air Cargo Challenge 2022 competition to ultimately achieve the optimal conceptual design decisions. It is based on the *OpenAeroStruct* framework, a low-fidelity aero-structural optimizer that uses the vortex-lattice method for the aerodynamic solver and a 1D truss, beam and torsional finite element for the structural solver. Additional capabilities were developed, namely a trajectory optimization module using a collocation method, with the option of using b-spline interpolation methods to increase optimizer efficiency. Two different propulsive models were also added to accurately determine the aircraft propulsive response to control input. Using gradient-based algorithms, the Air Cargo Challenge competition was studied using two methods: single score optimization and global score optimization. Optimization results showed that cargo carried is of the utmost importance along with the trajectory choice and the trimmed conditions of the aircraft in each flight segment. Trajectory optimization b-spline interpolation efficiency method revealed a decrease in computational time of 43% and a better optimizer response overall. The propulsive models showed the importance of accurately representing a system's behaviour.

Keywords: Trajectory optimization, Aerostructural design, Multidisciplinary design optimization, Optimization efficiency, Air Cargo Challenge

1. Introduction

Engineering is the source of most problem solutions nowadays, specially on aircraft design, where rigorous and complex systems are involved. Aircraft design is the search for the best solution for any air vehicle problem, which, in its foundation, is an optimization problem with hundreds of design variables and highly complex systems.

Three major subjects of optimization study are aerodynamics, structures and trajectory, which have many ramifications of their own. The aerodynamics field allows for the study of the best geometry in every component that is subjected to the air flow and in contact with it. Structures subject is the search for the lightest reliable structure possible, being its optimization highly focused on mass reduction. Finally, trajectory optimization searches for the best trajectory possible for the mission at hand which usually (not done in this work) tends to fuel burn minimization. The purpose of this work

is to couple all three disciplines in the search for the optimal conceptual design for the Air Cargo Challenge 2022 competition, a university UAV competition focused on payload, climb and cruise flight behaviour [1].

2. Theoretical Overview

2.1. Multidisciplinary Optimization

Multidisciplinary Optimization, or MDO, can be described as a collection of mathematical techniques for multi-variable optimization in which the optimization clearly crosses disciplinary boundaries simultaneously [2]. MDO can be built with different types of "architectures" - Monolithic and Distributed [3]. This work uses a Multidisciplinary Feasible (MDF) monolithic architecture which has the advantages of being, when compared to other monolithic architectures, the smallest optimization problem [3]. Figure 1 depicts an MDF architecture example approach for three disciplines in the form of an extended design structure matrix (XDSM) diagram [4].

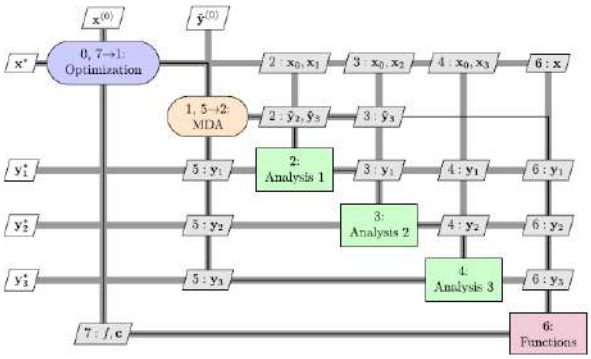

Figure 1: MDF architecture diagram with a Gauss-Seidel multidisciplinary analysis [3].

2.2. Computational Fluid Dynamics

Aerodynamics studies the body-fluid interactions and their products. For an aerodynamic analysis, one can choose between high or low fidelity methods. *OpenAeroStruct* (OAS), a highly efficient low fidelity optimizer, uses the Vortex Latice Method (VLM) as the aerodynamic solver [5]. This method models the wing as a combination of horseshoe vortices illustrated in Fig. 2, where each vortex filament of the horseshoe induces a flow field around its surrounding space.

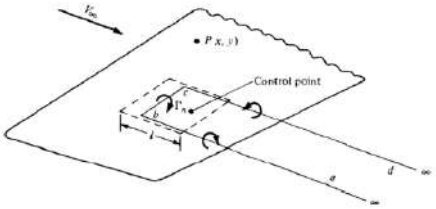

Figure 2: Example of a horseshoe vortex in a generic location of a wing surface [6].

The Biot–Savart [6] law relates the velocity of the flow field at an arbitrary point P caused by a segment dl of a vortex filament with circulation strength Γ, which integrated over a semi-infinite straight vortex filament, leads to

$$V = \frac{\Gamma}{4\pi h} = a\Gamma \quad , \tag{1}$$

where h is the distance from point P to the finite start point of the vortex filament and a the aerodynamic influence coefficient of the considered horseshoe panel to point P.

The VLM method will consist of spanwise and chordwise horseshoe panels that, by imposing flow tangency conditions in each panel, result in a linear system of equations of the form

$$[A][\Gamma] = \{\vec{V} \cdot \vec{n}\} \quad , \tag{2}$$

where $[A]$ is the aerodynamic influence coefficient matrix and $\vec{n}$ is the normal to the panel.

By solving this linear system of equations, the circulation of each panel is determined which in turn can be used to calculate the force acting in each panel as

$$\vec{F_i} = \rho\Gamma_i(\vec{V_\infty} + \vec{v_i}) \times \vec{l_i} \quad , \tag{3}$$

where $\vec{v_i}$ is the induced velocity at the center of the bound vortex, and $\vec{l_i}$ is the bound vortex vector.

2.3. Computational Structural Mechanics

Structures is the field where material mechanical behaviour is studied. OpenAeroStruct [6] offers two types of spars to model the structural behaviour of the wing: tubular spar and wingbox. This work uses a finite wingbox model (presented in Fig. 3) since it can provide lower weight solutions.

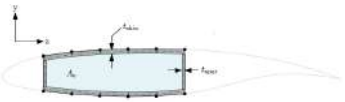

Figure 3: Typical wingbox section geometry scheme [7].

The structural model, formulated using the Finite Element Method (FEM) model, is a spatial beam element approach with six DOFs (degrees of freedom) per node as presented in Fig. 4. This element is a combination of truss, beam and torsional elements, which simultaneously carry axial, bending and torsional loads [6].

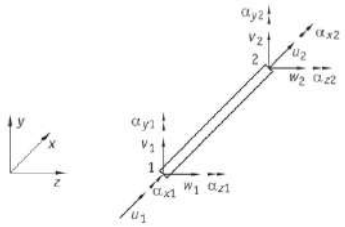

Figure 4: FEM element used for the structural model chosen [6].

The element comprises a 2 node system, with a total of 12 DOFs, where each node can translate in every direction (x, y and z) and can rotate in respect to all three axis (x, y and z), producing a 12×12 local stiffness matrix based on the wingbox sectional geometry and material properties [8]. The global stiffness matrix is assembled using transformed local stiffness matrices by applying transformation matrices to each local element to transform from local to global coordinates. Finally, the linear system of equations to be solved is

$$[K]\vec{u} = \vec{F} \quad , \tag{4}$$

where $[K]$ is the global stiffness matrix, $\vec{u}$ the displacement vector and $\vec{F}$ the forces. The forces result from the aerodynamic model, calculated for each wing section and applied to every structural element node.

2.4. Electric Propulsive System

Electric Propulsive System refers to the propulsive system of the aircraft, responsible for generating thrust. Usually a propulsion system involves a propulsive engager (thermal engine or electric motor) and a propulsive actuator (fan blades or propellers). The typical electrical propulsion system used in the environment of this work's purpose includes a motor (input energy), a propeller (output thrust), as electronic speed controller (ESC) and a battery (electrical storage).

This work uses experimental wind tunnel testing data to model the propulsive response to the control input. The operator chooses a certain control of thrust power (δ_t) that imposes a certain power consumption of the battery and consequently a power output from the brushless motor. Afterwards the propulsive model implemented uses this input power and calculates the thrust output of the system. Parallel to this, a calculation of energy consumption is processed.

2.5. Trajectory Optimization Methods

There are many techniques for numerically solving trajectory optimization problems [9], classified as either indirect or direct methods.

This work implements a direct collocation method which is considered powerful for solving general optimal control problems [9]. This method involves the parametrization of the trajectory into

state and control variables and solving implicit or explicit numerical integration equations while respecting several constraints - the defects. These are the result of the dynamics of the problem. The defects represent the disparity metric of the differential equations.

This formulation starts by dividing all variables defined for the trajectory, which are a function of time, in finite intervals of time and describing them in a polynomial manner of a specific degree in each interval. In each interval, a numerical integration method is used to calculate the defects value and a constraint is used to verify if the defects respect their expected null value. The optimization can be initialized to maximize or minimize a certain objective and the trajectory's state and control variables will be "collocated" into their optimum values while respecting every constrained added to the problem and always their defects. In this work, a trapezoidal direct collocation method is used as

$$x_{k+1} - x_k = \frac{1}{2}(t_{k+1} - t_k)(v_{k+1} + v_k) \quad . \qquad (5)$$

3. Implementation

3.1. B-spline Trajectory Model

The trajectory model implemented uses b-spline interpolation functions to create a curve that fits the dynamics criteria defined by the system with fewer control points than the number of steps used to verify the system's dynamics. Figure 5 shows the visual explanation of the aforementioned.

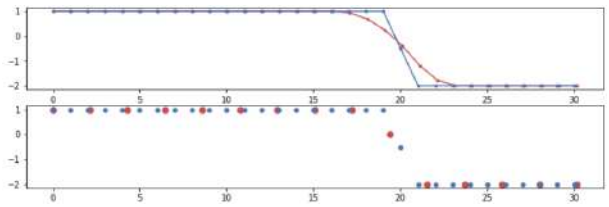

Figure 5: B-spline approach and control point visualization compared with unmodified direct collocation control point mechanism.

3.2. Propulsion Models

Through wind-tunnel analyses, two models are implemented: constant power and decay power. Constant power results from the assumption of a non-decay power source. Decay power model includes the battery's voltage decay through time with a model based on battery capacity levels. The more complex and accurate model is presented in Fig. 6.

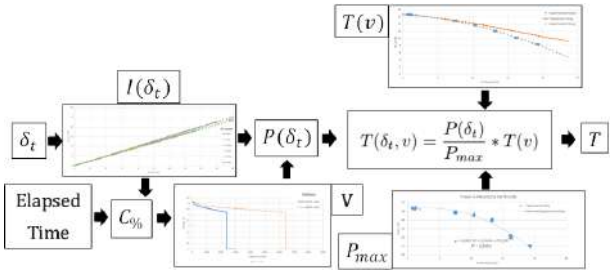

Figure 6: Propulsion model for a modelled discharge battery.

3.3. Competition and Flight Related Models

To better evaluate the problem at hand, several models are implemented into the framework. These include a cargo bay parasite drag prediction model, a rhombus box model and stability model. The cargo bay parasite drag prediction model (see Fig. 7) is calculated depending on the expected payload carried by the aircraft, which models the cargo bay in an $m \times n$ manner, where n describes the number of upward blood bag lines and m the described the number of possible lined-up bags.

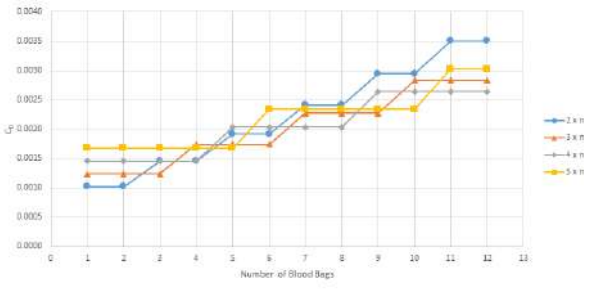

Figure 7: Cargo bay parasite drag estimation for different blood bag arrangements.

The rhombus box model, follows the ACC 2022

rules [1], where it is stated that the aircraft must fit inside a quadrilateral geometry with equal sides where the inner angle β can be freely modified. To model the geometric references presented in Figure 8 are created, where each quantity presented is constrained to be positive.

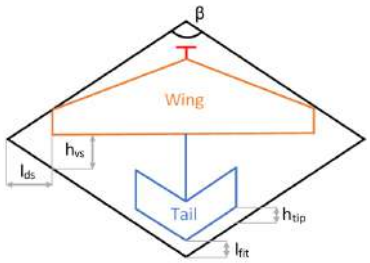

Figure 8: General configuration for the rhombus box model used.

As for the equilibrium and stability model, a trimmed condition is used where the pitch moment in each collocation points must be null and a vertical tail volume constraint to dimension the vertical component of the "V" tail design.

3.4. Framework Architecture

The created framework comprises three major elements: Problem variables, which include all state, control, geometric and auxiliary variables for the problem's trajectory and aircraft; Mission points calculations, which involves wing geometric variables definition, the aero-structural coupling as well as the propulsion calculations and all the needed pre-calculations; Mission performance and constraints, in which the needed measurements are taken to evaluate the aircraft performance. The overall optimization scheme is presented in Fig. 9 where a XDSM [4] diagram is depicted describing the whole framework.

4. Results

This work comprises four different analyses: Single solutions, Coupled design and trajectory optimization, B-spline interpolation efficiency and Thrust model comparison. The first comprises a direct approach of the framework built for the three score independent cases of the competition - payload, climb and distance. The second delivers an in-depth analysis of the pursuit of the optimal conceptual design. Finally, the last two sections analyse the influence of the b-spline method implemented and the comparison of the propulsion models.

4.1. Single Optimization

Single segment optimization comprises the direct application of the framework capabilities considering each score segment function. These represent a portion of the total score and are described as

$$S_{payload} = 1000\frac{P_{team}}{P_{max}} \tag{6a}$$

$$S_{climb} = 1000\frac{PS_{altitude,team}}{PS_{altitude,max}} \tag{6b}$$

$$S_{distance} = 1000\frac{D_{team}}{D_{max}} \tag{6c}$$

where P_{team}, P_{max}, $PS_{altitude,team}$, $PS_{altitude,max}$, D_{team} and D_{max} represent the payload of the team, maximum payload achieved overall in the competition, pre-score altitude of the team, maximum pre-score altitude achieved overall in the competition, distance travelled by the team and maximum distance achieved in a 120 seconds flight overall in the competition, respectively. The pre-score altitude is calculated as

$$PS_{altitude} = -3.92e^{-5}h_{60s}^4 + 1.08e^{-2}h_{60s}^3 - 1.156h_{60s}^2 + 64.2h_{60s} - 537 \tag{7}$$

where h_{60s} is the altitude achieved in 60 seconds of climb.

The initial flight profile along with the initial geometry (Fig. 10) were intended to be sub-optimal to promote the framework to search for the optimal solution.

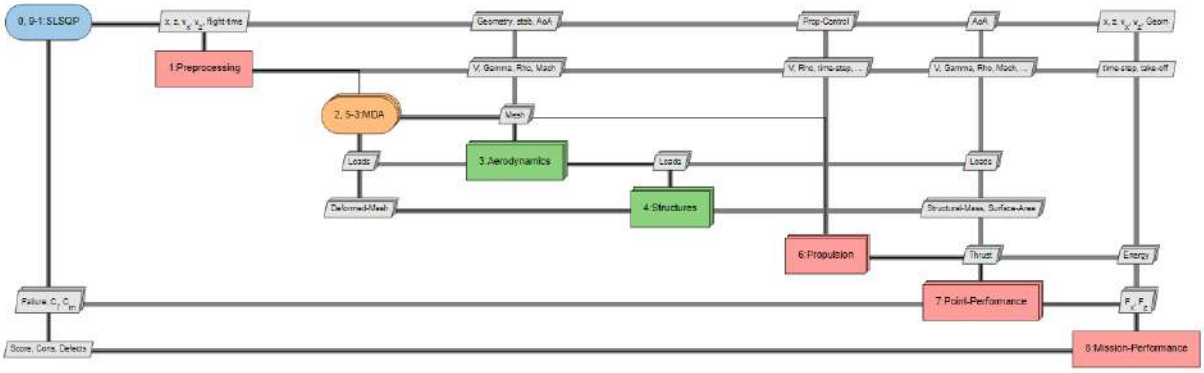

Figure 9: XDSM diagram for the created framework. Created with [10]

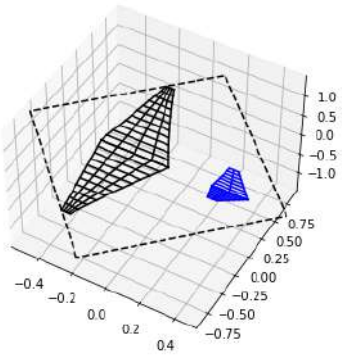

Figure 10: Aircraft initial configuration.

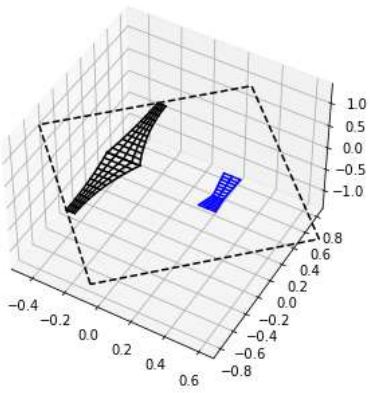

Figure 11: Aircraft climb optimized planform.

Climb optimized configuration (Fig. 11) resulted in a light weight (1.3kg compared to the usual 2kg) solution where the trajectory chosen maximized the climb achieved at the 60 seconds mark. Although the climb solution was not the best, the optimization's search path is in correlation with the purpose of this single objective formulation. Additionally, it was observed that the distance travelled for this solution is also high.

As for the distance segment optimization (Fig. 12), the configuration achieved is very similar to the one achieved through optimizing the climb, but with different trajectory choices. Unexpectedly however, the thrust response (Fig. 13) showed a sub-optimal choice. This result evidences other factors that play a role in this problem: higher thrust implies higher lift that ultimately changes the aircraft's trim condition, leading to a higher elevation, which is not permitted by the maximum altitude constraint of the competition [1].

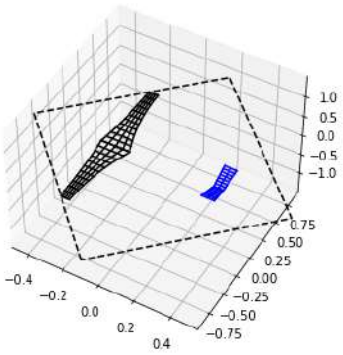

Figure 12: Aircraft distance optimized planform.

Lastly, in the payload optimization (Fig. 14), the framework sought, as expected, a higher surface area wing (0.72m^2 compared to the initial 0.39m^2) to maximize its lift and a loss in speed.

The final results are presented in Tab. 1. The highest score total configuration is the payload one.

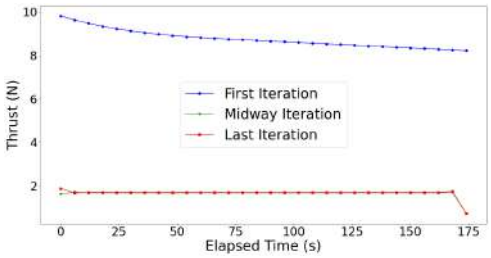

Figure 13: Aircraft thrust.

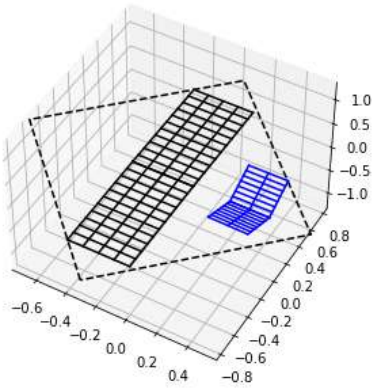

Figure 14: Aircraft payload optimization planform.

This happens due to the payload effect on the score. While no payload leads to no score points in the payload segment, a heavier slower aircraft still earns a good amount of score points in both climb and distance parts.

4.2. Coupled Design and Trajectory Optimization

For the coupled design and trajectory optimization, the final score function was used,

$$S_{total} = (S_{distance} + S_{climb} + S_{payload}) \times (1 + P_{to\_bonus}) \quad (8)$$

where P_{to_bonus} represents the take-off bonus and can assume either the value of 0 or 0.1 depending on the take-off distance (0.1 for a runway equal or less than 40m).

Three different case studies were analysed: the same initial configuration as the previous individual segment studies (#1); a more defined wing shape initial solution with the same initial trajectory but a better climb performance (#2); and an initial solution with a bound restriction for the wing span of 1.8m, to study boundary influence (#3). Each optimization result is presented in Figs. 15, 16 and 17.

The best set of overall metrics of the aircraft in each optimization are presented in Tabs. 2 and 3. These geometric results indicate three major aspects of the wing geometric preferences for the optimized solutions: (i) the wing area is relatively high; (ii) the sweep is preferred close to null values and (iii) the wing chord is kept at the maximum.

All three studied cases present close to maximum chord values, which reveals that for all optimization cycles, the chord was maximized for the achieved wing span, which represents the wing surface area maximization for a fixed optimized span. Additionally, the thickness of the wing is kept in average at low values, which benefits a faster aircraft and increases the climb and distance score points while maintaining high wing area.

As for the tail, sweep is kept close to null or negative and the area is kept between 15 to 20 % of the wing area. Additionally, the dihedral for the first two cases is lower and higher for the last one.

As for the trajectory, results are depicted in Fig. 18, where only the case study #1 results are presented for reference. The optimized results focus on climbing to maximize the climb score and, afterwards, focus on increasing the speed to increase the distance score.

As for the propulsion, Fig. 19 presents the thrust results for case study #3 for reference. The most effort is produced in the climb segment and the cruise segment is less demanding for the propulsion system. Additionally, low throttle values are observed for the cruise segment. This indicates the cruise flight can be further optimized to achieve a trimmed configuration with higher throttle and speed while

Table 1: Score points for each optimization.

	Climb Score	Distance Score	Payload Score	Total Score
Climb Optimization	943.6	929.4	83.3	2151.9
Distance Optimization	638.8	930.1	0 .0	1725.8
Payload Optimization	615.5	656.3	750.0	2224.0

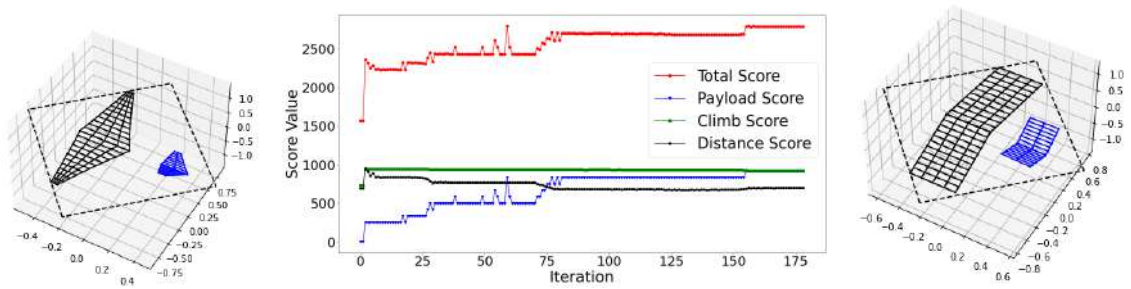

(a) Initial configuration. (b) Score progression. (c) Optimized configuration.

Figure 15: Aircraft visual results for case study #1.

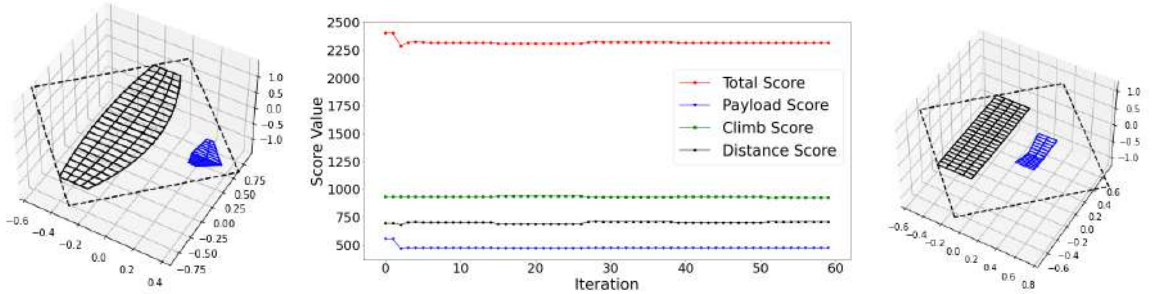

(a) Initial configuration. (b) Score Progression. (c) Optimized configuration.

Figure 16: Aircraft visual results for case study #2.

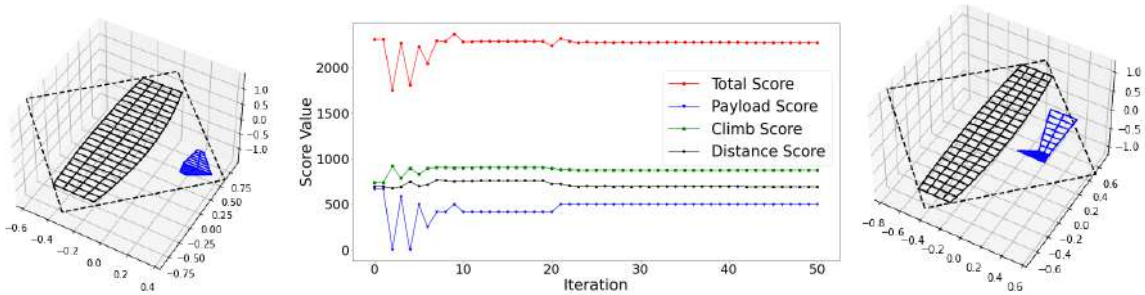

(a) Initial configuration. (b) Score progression. (c) Optimized configuration.

Figure 17: Aircraft visual results for case study #3.

maintaining similar climb behaviour.

4.3. B-Spline Interpolation Usage

To study the performance influence of global b-spline interpolation usage, a study was conducted based on a fixed set of control points using case study #3 as comparison. The results are presented in Tab. 4.

Clearly, the b-spline method implemented not only increases the obtained score value by more than 4%, but also decreases the computational time by almost 43%. Additionally, by representing each state and control variable by interpolating func-

Table 2: Wing conceptual design metrics for all case studies.

Wing				
	#1	#2	#3	Average
$\overline{c_w}$ [m]	0.40	0.37	0.37	0.38
S_w [m^2]	0.72	0.43	0.68	0.61
AR_w	4.51	3.18	5.06	4.25
Λ_w [°]	1.01	0.00	0.07	0.36
t/c_w	0.08	0.08	0.12	0.09
λ_w	1.00	0.98	0.77	0.92

Table 3: Tail conceptual design metrics for all case studies.

Tail				
	#1	#2	#3	Average
S_t [m^2]	0.15	0.08	0.10	0.11
Λ_t [°]	-0.14	0.00	-0.09	-0.08
τ_t [°]	35.23	35.04	59.68	43.32

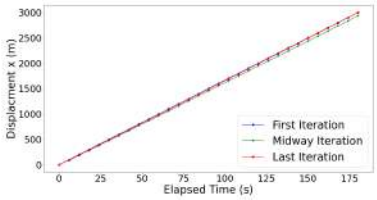

(a) Case #1 aircraft x displacement.

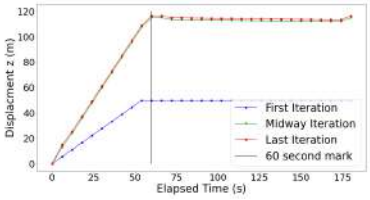

(b) Case #1 aircraft z displacement.

Figure 18: Trajectory results for all case studies.

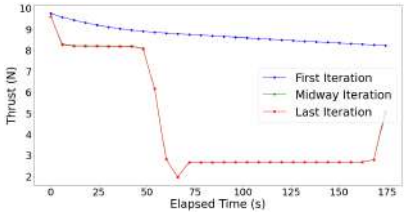

Figure 19: Thrust results for case study #3.

tions, this method created more realistic smooth function curves that are closer to the aircraft's real scenario.

Table 4: Control points used for global influence analysis of the b-spline interpolation method based on case study #3.

	x	$\dot{x}$	z	$\dot{z}$	δ_t	δ_{stab}
CP	20	20	25	25	10	20

Score	2374.5	Score Δ%	4.33
Comp time (s)	4186.9	Comp time Δ%	-42.73

4.4. Thrust Model Comparison

To study thrust model difference, case study #3 was again used with both formulated methods. Both optimizations started with the same initial configuration and the propulsive response is presented Fig. 20.

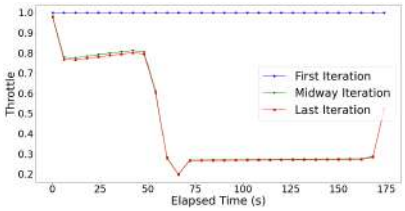

(a) Decay power model throttle results.

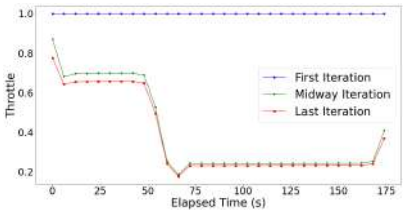

(b) Constant power model throttle results.

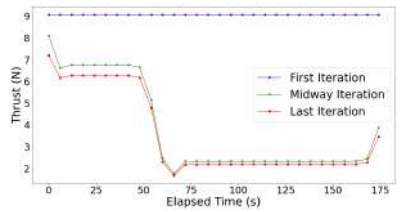

(c) Constant power model thrust results.

Figure 20: Propulsion system results for both implemented propulsive models.

Comparing these, the thrust curves are almost identical, however the throttle curves are different. For the decay battery model, the throttle input must be corrected to a non-constant curve to perform a constant curve for the thrust curve. On the other hand, for the constant power model, the

throttle and thrust curves have a linear correspondence.

5. Conclusions

In this work, a framework was developed to study the ACC 2022 competition optimal conceptual design. The ACC 2022 optimal design characteristics were determined based on different singular and global case studies. Coupled design and trajectory optimizations were conducted leading to the following conclusions: (i) climb maximum height is possible to achieve and should be the focus of the first sixty seconds of flight; (ii) the wing area should be maximized within the bounded limits to maximize cargo; (iii) tail and wing geometries follow similar tendencies in all optimization cases, which helps defining a optimal conceptual region; (iv) to maximize travelled distance, trim conditions should be carefully analysed to assure a near maximum thrust condition on the cruise part.

The b-spline interpolation model implemented resulted in better search paths for the optimizer and a 43% computational efficiency gain. Propulsive models implemented showed that non-realistic models can produce better but unrealistic results.

References

[1] Air cargo challenge 2022 participation handbook, March 2021. version 01.11.

[2] Daniel P. Raymer. *Enhancing Aircraft Conceptual Design Using Multidisciplinary Optimization.* PhD thesis, Royal Institute of Technology, May 2002. ISBN 91-7283-259-2.

[3] Joaquim Martins and Andrew Lambe. Multidisciplinary design optimization: A survey of architectures. *AIAA Journal*, 51:2049–2075, 2013.

[4] Andrew Lambe and Joaquim Martins. Extensions to the design structure matrix for the description of multidisciplinary design, analysis, and optimization processes. *Structural and Multidisciplinary Optimization*, 49:273–284, 2012.

[5] Jonh Anderson. *Fundamentals of Aerodynamics.* McGraw-Hill Education, 6^{th} edition, 2016. ISBN-13: 978-1259129919.

[6] John P. Jasa, John T. Hwang, and Joaquim R. R. A. Martins. Open-source coupled aerostructural optimization using python. *Structural and Multidisciplinary Optimization*, 57:1815–1827, 2018.

[7] Shamsheer S. Chauhan and Joaquim R. R. A. Martins. Low-fidelity aerostructural optimization of aircraft wings with a simplified wingbox model using OpenAeroStruct. In *Proceedings of the 6th International Conference on Engineering Optimization, EngOpt 2018*, pages 418–431, Lisbon, Portugal, September 2018. Springer.

[8] Giovanni Zucco, Vincenzo Oliveri, Mohammad Rouhi, Robert Telford, Daniël Peeters, Gearoid Clancy, Ciarán McHale, Ronan O'Higgins, Trevor Young, and Paul Weaver. Static test of a variable stiffness thermoplastic composite wingbox under shear, bending and torsion. *Aeronautical Journal -New Series-*, 124, 2019.

[9] John T. Betts. Survey of numerical methods for trajectory optimization. *Journal of Guidance, Control, and Dynamics*, 21(2):193–207, 1998.

[10] Rémi Lafage, Sebastien Defoort, and Thierry Lefebvre. Whatsopt: a web application for multidisciplinary design analysis and optimization. In *AIAA Aviation 2019 Forum*, page 2990, 2019.